Applied Catalysis B: Environmental 144 (2014) 885–892

Contents lists available at ScienceDirect

Applied Catalysis B: Environmental

journal homepage: www.elsevier.com/locate/apcatb

Synthesis and characterization of g-C_3N_4/Ag_3VO_4 composites with significantly enhanced visible-light photocatalytic activity for triphenylmethane dye degradation

Shaomang Wang[a,b], Dinglong Li[b], Cheng Sun[a,*], Shaogui Yang[a], Yuan Guan[b], Huan He[a]

[a] State Key Laboratory of Pollution Control and Resource Reuse, School of the Environment, Nanjing University, Nanjing 210023, PR China
[b] School of Environment and Safety Engineering, Changzhou University, Changzhou 213164, PR China

ARTICLE INFO

Article history:
Received 10 May 2013
Received in revised form 31 July 2013
Accepted 6 August 2013
Available online 18 August 2013

Keywords:
G-C_3N_4/Ag_3VO_4
Photocatalytic degradation
Triphenylmethane dyes
Degradation mechanism

ABSTRACT

The g-C_3N_4/Ag_3VO_4 hybrid photocatalysts were prepared by Ag_3VO_4 anchoring on the surface of g-C_3N_4. The transmission electron microscope, X-ray diffraction, Fourier transform infrared spectroscopy and X-ray photo-electron spectroscopy analyses demonstrated that Ag_3VO_4 nanoparticles well distributed on the surface of g-C_3N_4 and the g-C_3N_4/Ag_3VO_4 hetero-junctions were formed. Compared with pure g-C_3N_4 and Ag_3VO_4, the g-C_3N_4/Ag_3VO_4 hybrid materials displayed much higher photocatalytic activity for basic fuchsin degradation (20 mg/L, 50 mL) under visible-light irradiation. The 40 wt% g-C_3N_4/Ag_3VO_4 photocatalyst exhibited optimal removal rate constant of 0.92 h^{-1}, which was 11.5 and 6.6 times higher than that of pure g-C_3N_4 and Ag_3VO_4, respectively. Density functional theory calculations indicated that complementary conduction and valence band-edge hybridization between g-C_3N_4 and Ag_3VO_4 could apparently increase separation efficiency of electron-hole pairs of g-C_3N_4/Ag_3VO_4 composites, which was confirmed by photoluminescence spectra. In addition, it was found that h^+ and $\bullet O_2^{-1}$ generated in the photocatalytic process played a key role in basic fuchsin degradation.

© 2013 Elsevier B.V. All rights reserved.

1. Introduction

Industrial wastewaters, especially such as tannery and textile processing effluents, are often detected containing a high content of dissolved organic dyes, which are usually hazardous to organisms [1,2]. At present, removal of organic dyes from wastewater is a serious challenge faced by human beings. To address this challenge, many technologies of organic dye degradation such as chemical oxidation, physical adsorption and biodegradation have been developed. However, these technologies still have some problems such as secondary pollution or unsatisfactory treatment. Lately, photocatalytic applied in organic pollutant removal has caused much attention due to the utilization of abundant solar energy without the need for additional chemical regents. Hence, many types of semiconductor photocatalysts such as TiO_2 [3–5], ZnO [6] and $BiPO_4$ [7] were successfully prepared by a variety of methods. To date, TiO_2 is still the most widely investigated semiconductor photocatalytic material owning to high activity under UV irradiation. But UV light only accounts for no more than 4% of the solar spectrum, which limits its practical application for environmental remediation. To effectively harness abundant natural sunlight, many visible-light-driven photocatalysts such as $BiVO_4$ [8,9], Bi_2WO_6 [10], BiOI [11–13] and Ag_3PO_4 [14,15], etc. were also successfully developed.

Recently, a novel visible-light catalytic material, graphitic carbon nitride (g-C_3N_4) has been fabricated from cyanamide [16]. G-C_3N_4 is a nontoxic metal-free semiconductor that possesses outstanding thermal, electrical and optical characteristics [17]. These unique properties have attracted a great deal of scientific interest, specially its potential applications in producing hydrogen or oxygen of water splitting and organic pollutant degradation [18–20]. However, g-C_3N_4 has some disadvantages such as small surface area and low quantum efficiency [21], both of which lead to low photocatalytic activity. Therefore, enhancing photocatalytic activity of g-C_3N_4 needs further study. Semiconductor Ag_3VO_4 reported by Konta et al. showed some visible-light catalytic activity for water splitting into H_2 and O_2 [22]. Nevertheless, the photocatalytic activity of pure Ag_3VO_4 is still low and requires to be further modified. To the best of our knowledge, there are no reports on catalytic performance of Ag_3VO_4 being improved by g-C_3N_4 doping. The Ag_3VO_4 hybridized with g-C_3N_4 might produce a high-performance photocatalytic material for organic pollutant removal.

In this study, the g-C_3N_4/Ag_3VO_4 hybrid photocatalysts were prepared by a facile precipitation method. The photocatalytic performances of the catalysts were evaluated by decomposing hazardous triphenylmethane dyes such as basic fuchsin (BF), malachite

* Corresponding author. Tel.: +86 25 89680258; fax: +86 25 89680580.
E-mail address: envidean@nju.edu.cn (C. Sun).

0926-3373/$ – see front matter © 2013 Elsevier B.V. All rights reserved.
http://dx.doi.org/10.1016/j.apcatb.2013.08.008

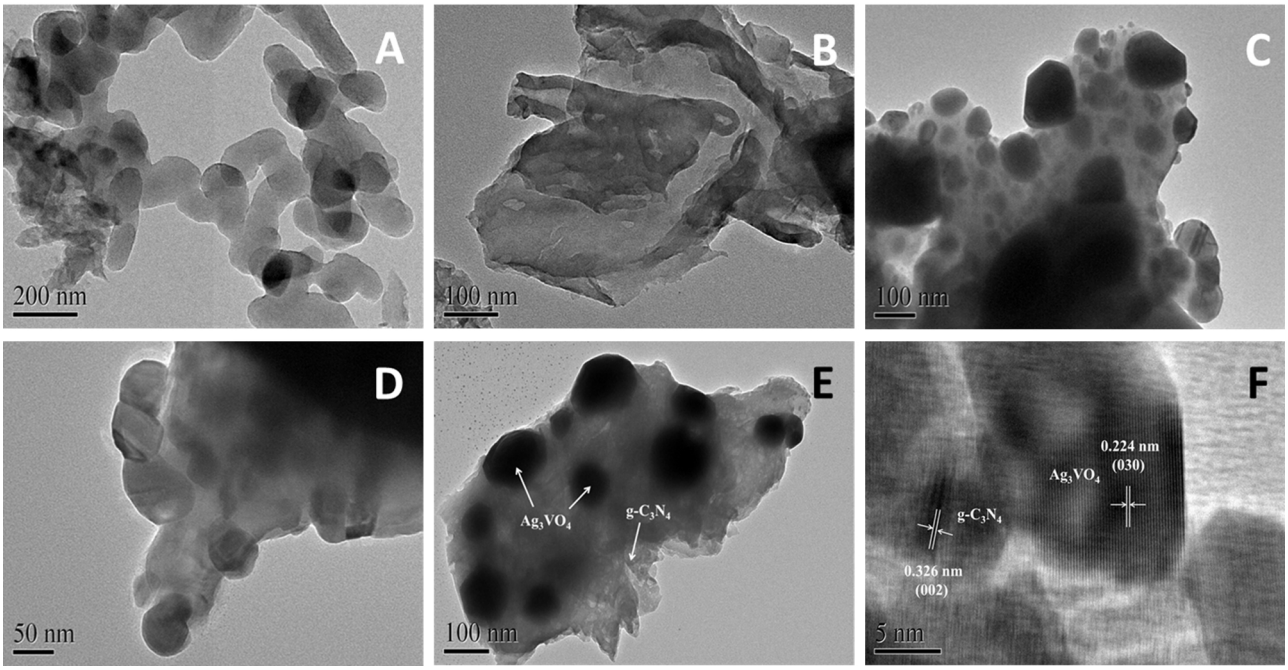

Fig. 1. TEM images of g-C_3N_4 (A and B), Ag_3VO_4 (C and D), 40 wt% g-C_3N_4/Ag_3VO_4 (E). HRTEM image of 40 wt% g-C_3N_4/Ag_3VO_4 (F).

green (MG) and crystal violet (CV) in water under visible-light irradiation. The mechanism of enhanced photocatalytic activity of g-C_3N_4/Ag_3VO_4 composites was investigated. The reactive species for the dye degradation were determined.

2. Experimental

2.1. Preparation of g-C_3N_4/Ag_3VO_4 hybrid materials

All starting materials in the experiment were purchased commercially and used without further purification.

Graphitic carbon nitride (g-C_3N_4) was prepared by directly heating melamine in a program-controlled tubular furnace according to the literature [16]. Typically, 10 g of melamine was placed into a semi-closed combustion boat, which was heated at a rate of 3 °C min^{-1} to reach 550 °C and then was calcined at this temperature for 2 h in a flowing nitrogen atmosphere. After the tubular furnace was naturally cooled to room temperature, g-C_3N_4 was obtained in the form of yellow powders.

The g-C_3N_4/Ag_3VO_4 composites were synthesized by Ag_3VO_4 anchoring on the surface of g-C_3N_4 (Fig. S1). The typical procedure was as follows: 0.22 g of g-C_3N_4 was dispersed in 55 mL of H_2O by ultrasonication for 0.5 h. Subsequently, 2.55 g of $AgNO_3$ was added into the solution and then the mixture was magnetically stirred for 0.5 h. Next, 40 mL of aqueous solution containing 2 g of $Na_3VO_4 \cdot 12H_2O$ was slowly dropped into the above suspension and reacted by magnetic stirring for 4 h. Finally, the resulting precipitate was washed by deionized water and dried at 90 °C to obtain 10 wt% g-C_3N_4/Ag_3VO_4. Other g-C_3N_4/Ag_3VO_4 hybrid materials with different g-C_3N_4 content were prepared by the similar method.

2.2. Characterization

Transmission electron microscope images were obtained from JEM-200CX (JEOL, Japan). The crystalline phases of as-prepared

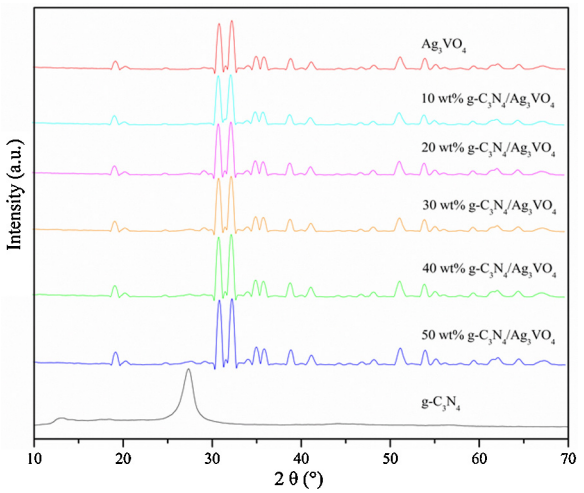

Fig. 2. XRD patterns of g-C_3N_4, Ag_3VO_4 and g-C_3N_4/Ag_3VO_4 composites.

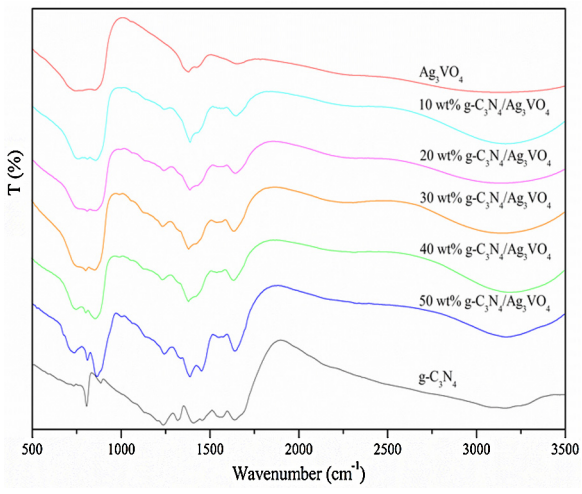

Fig. 3. FT-IR spectra of g-C_3N_4, Ag_3VO_4 and g-C_3N_4/Ag_3VO_4 hybrid materials.

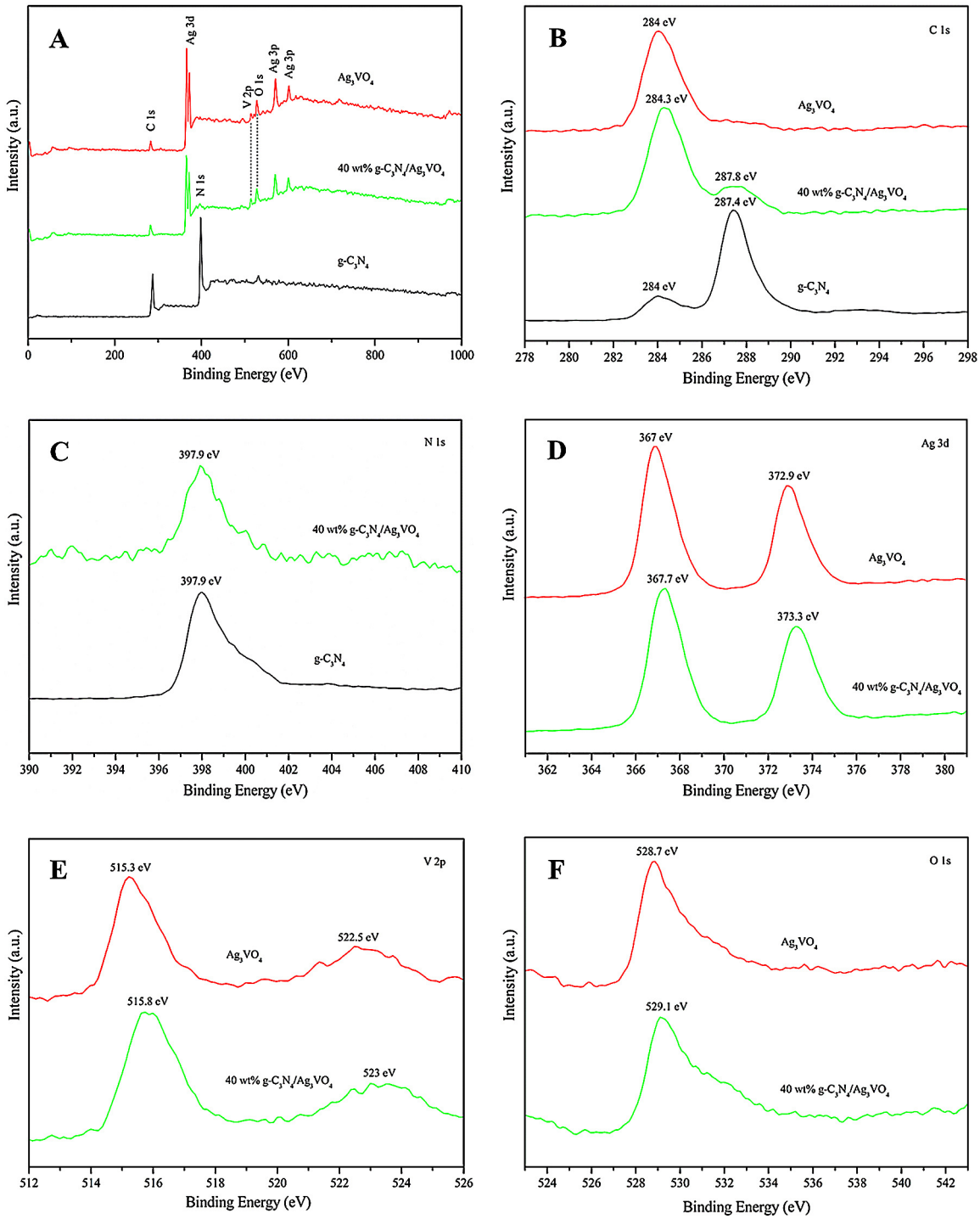

Fig. 4. XPS spectra of the samples: (A) the survey scan and (B) C 1 s of g-C_3N_4, Ag_3VO_4 and 40 wt% g-C_3N_4/Ag_3VO_4; (C) N1s of g-C_3N_4 and 40 wt% g-C_3N_4/Ag_3VO_4; (D) Ag 3d, (E) V 2p and (F) O 1s of Ag_3VO_4 and 40 wt% g-C_3N_4/Ag_3VO_4.

photocatalysts were determined by a diffractometer with Cu *Kα* radiation (Model, Shimadzu LabX XRD-6000). The Fourier transform infrared spectroscopy (FT-IR) spectra were recorded by NEXUS870 (NICOLET, USA). X-ray photo-electron spectroscopy (XPS) was used to identify surface chemical composition and chemical states of the catalysts on a PHI5000 Versa Probe electron spectrometer using Al *Kα* radiation (ULVAC-PHI, Japan). The UV–vis diffuse reflectance spectra (DRS) were measured using a spectrophotometer (Shimadzu UV2550) with $BaSO_4$-coated integrating sphere in the wavelength range of 300–800 nm. The Photoluminescence (PL) spectra of the catalysts were collected by Fluoromax-4 (HORIBA, USA) with an excitation wavelength at 350 nm. Total organic carbon (TOC) was analyzed by TOC measuring instrument (Shimadz TOC-5000).

2.3. Photocatalytic reaction

The photocatalytic activities of as-synthesized photocatalysts were evaluated by decomposing basic fuchsin (BF), malachite green (MG) and crystal violet (CV) under visible-light irradiation in a photoreaction apparatus. Visible light (420 nm < λ < 700 nm) was generated by using 500 W Xe lamp irradiation with a 420 nm

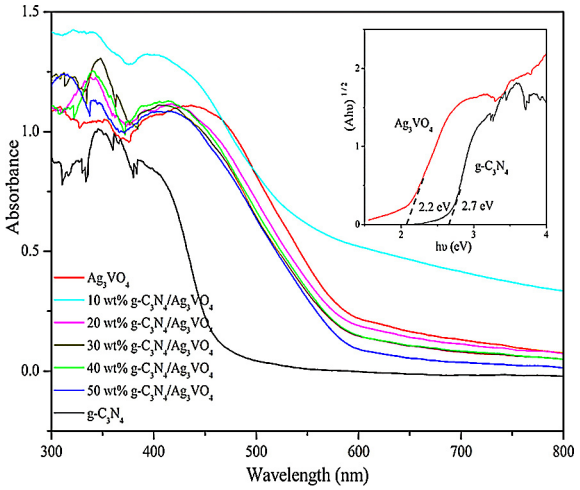

Fig. 5. UV–vis diffuse reflectance spectra of g-C_3N_4, Ag_3VO_4 and g-C_3N_4/Ag_3VO_4 composites.

cut-off filter to remove light of $\lambda < 420$ nm. For photodegradation of the dyes, 0.05 g of photocatalysts were put into 50 mL (20 mg/L) dye solutions. Prior to irradiation, the suspensions were magnetically stirred for 1 h to reach adsorption–desorption equilibrium in the dark. At given time intervals of visible-light irradiation, about 3 mL aliquots were collected and centrifuged to remove catalyst particles for analyses. The concentration of the dyes were determined by UV–vis spectroscopy at its maximum absorption wavelength.

3. Results and discussion

3.1. Characterization of photocatalysts

Fig. 1 shows the morphology of g-C_3N_4, Ag_3VO_4 and 40 wt% g-C_3N_4/Ag_3VO_4 by TEM. From Fig. 1A and B, a wrinkled-layer structure with several stacking layers could be clearly seen in the g-C_3N_4 sample, which was in line with the literature report [23]. The Ag_3VO_4 sample displayed a brick-like shape structure with a diameter of 50–100 nm (Fig. 1C and D). Two types of materials were found in the 40 wt% g-C_3N_4/Ag_3VO_4 (Fig. 1E), which corresponded to Ag_3VO_4 and g-C_3N_4, respectively. In addition, it was observed that the Ag_3VO_4 nanoparticles anchored on the surface of g-C_3N_4 and were well dispersed. HRTEM image of the composite further reveals interfacial interaction between Ag_3VO_4 and g-C_3N_4 (Fig. 1F). The lattice spacing of 0.224 nm matched with the d value of (030) crystal plane of Ag_3VO_4, whereas the interplanar spacing of 0.326 nm corresponded to distance between adjacent (002) crystal plane of g-C_3N_4 [16].

The crystal structures of as-synthesized photocatalysts were determined by XRD (Fig. 2). For g-C_3N_4, one strong peak was observed at 27.4°, which was in good accord with characteristic interplanar staking peak of aromatic systems [24]. The diffraction peaks of Ag_3VO_4 matched with its monoclinic phase (JCPDS No. 43–0542). The main characteristic diffraction peaks of g-C_3N_4/Ag_3VO_4 hybrid materials did not obviously change after Ag_3VO_4 hybridized with g-C_3N_4. No typical crystalline of g-C_3N_4 appeared in the g-C_3N_4/Ag_3VO_4 composites (g-C_3N_4/Ag_3VO_4 < 30 wt%). However, with increasing g-C_3N_4 content, the weak diffraction peak of g-C_3N_4 could be found. The results verified co-existence of g-C_3N_4 and Ag_3VO_4 in the g-C_3N_4/Ag_3VO_4 hybrid materials.

Fig. 3 shows the FT-IR spectra of as-fabricated photocatalysts. For FT-IR spectrum of g-C_3N_4, the absorption peaks at 1238, 1319, 1408, 1570 and 1641 cm^{-1} were observed, which were ascribed

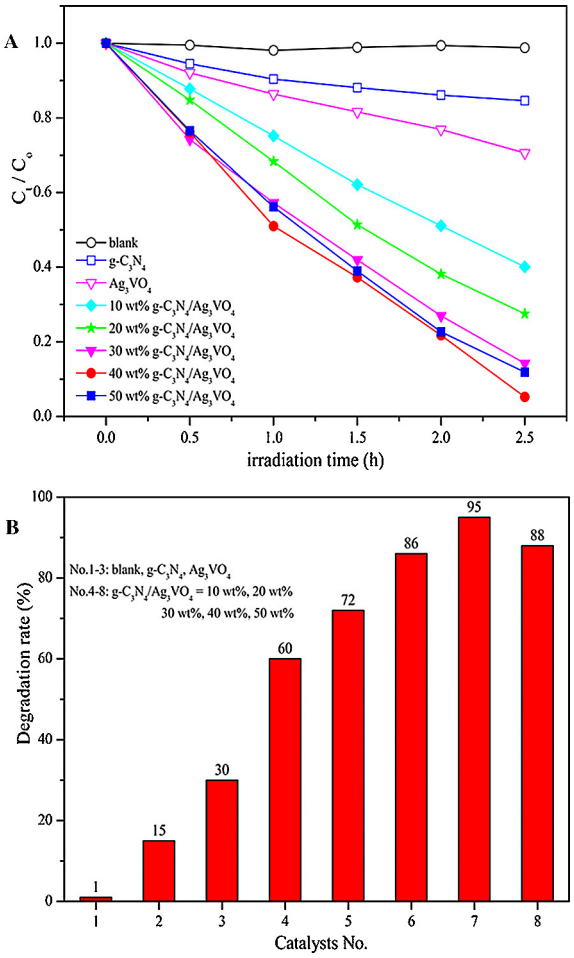

Fig. 6. Photocatalytic activities of as-prepared photocatalysts for BF degradation under visible-light irradiation (A). Degradation rate of BF after 2.5 h irradiation with visible-light (B).

to the C=N and C—N stretching vibration modes, respectively. The peak at 806 cm^{-1} was associated with the characteristic breathing mode of s-triazine [25]. For g-C_3N_4/Ag_3VO_4, with the increase of g-C_3N_4 content, the characteristic peaks of g-C_3N_4 could be clearly seen in the g-C_3N_4/Ag_3VO_4 composites, which further testified the XRD results.

The surface chemical composition of g-C_3N_4, Ag_3VO_4 and 40 wt% g-C_3N_4/Ag_3VO_4 and the interaction of g-C_3N_4 with Ag_3VO_4 were analyzed by XPS. In Fig. 4A, the survey scan XPS spectra provided C 1s and N 1s peaks for g-C_3N_4 and 40 wt% g-C_3N_4/Ag_3VO_4, as well as Ag 3d, V 2p and O 1s peaks for Ag_3VO_4 and 40 wt% g-C_3N_4/Ag_3VO_4, which was consistent with chemical composition of the photocatalysts. As shown in the high resolution XPS spectra of C 1s (Fig. 4B), one peak at 284 eV was observed in the Ag_3VO_4 sample, which belonged to external carbon contamination. In the case of g-C_3N_4, two carbon peaks at 284 eV and 287.4 eV were found, respectively. The first peak was assigned to external carbon atoms depositing on its surface [19,26]. The second peak was related to coordination between carbon atoms and three nitrogen atoms in the g-C_3N_4 lattice [27]. The 40 wt% g-C_3N_4/Ag_3VO_4 hybrid material also displayed two C 1s peaks at 284.3 eV and 287.8 eV, respectively, which were higher than binding energies of pure g-C_3N_4. It was due to the fact that Ag_3VO_4 hybridized with g-C_3N_4 resulted in inner shift of C 1s orbit. The N 1s peak of g-C_3N_4 and 40 wt% g-C_3N_4/Ag_3VO_4 was observed at 397.9 eV in Fig. 4C, which originated from C=N—C coordination [18]. In addition, N 1s maintaining the same binding energy suggested that a suitable

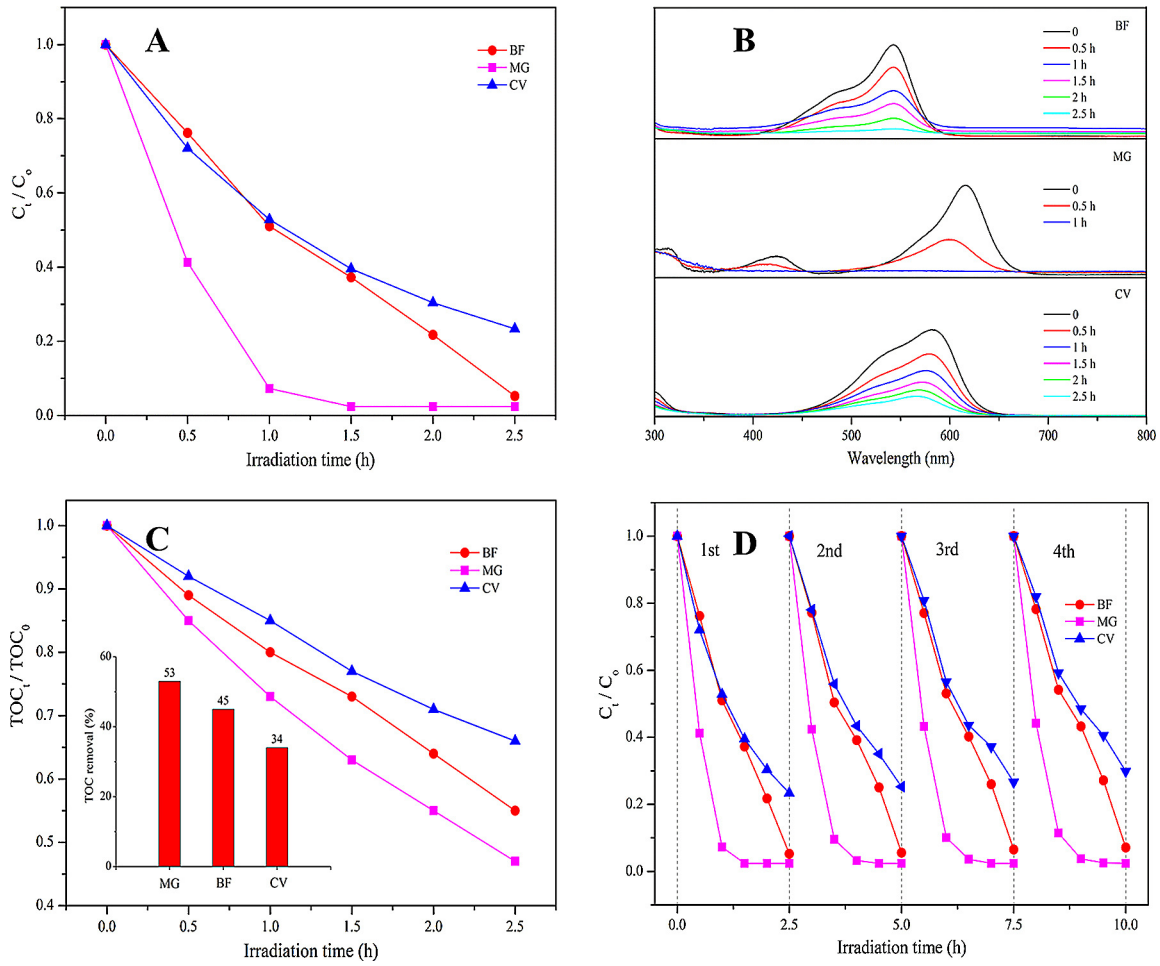

Fig. 7. Photocatalytic activity of 40 wt% g-C_3N_4/Ag_3VO_4 for BF, MG and CV degradation under visible-light irradiation (A). Temporal absorption spectral pattern (B) and TOC removal (C) of BF, MG and CV by 40 wt% g-C_3N_4/Ag_3VO_4. Four recycling runs of 40 wt% g-C_3N_4/Ag_3VO_4 for BF, MG and CV degradation (D).

combination of g-C_3N_4 and Ag_3VO_4 inducing N 1s orbit offset could be ruled out. The Ag 3d peaks of Ag_3VO_4 located at 367 eV and 372.9 eV (Fig. 4D), which corresponded to the Ag 3d 5/2 and Ag 3d 3/2 binding energies. However, the binding energies of Ag 3d 5/2 and Ag 3d 3/2 of 40 wt% g-C_3N_4/Ag_3VO_4 were 367.7 eV and 373.3 eV, which were higher than that of pure Ag_3VO_4. A similar phenomenon was also found in the XPS spectra of V 2p (Fig. 4E) and O 1s (Fig. 4F). The binding energies of V 2p 3/2 (515.8 eV), V 2p 1/2 (523 eV) and O 1s (529.1 eV) of 40 wt% g-C_3N_4/Ag_3VO_4 were higher than that of V 2p 3/2 (515.3 eV), V 2p 1/2 (522.5 eV) and O 1s (528.7 eV) of pure Ag_3VO_4. Such results could be similarly attributed to the interaction of g-C_3N_4 with Ag_3VO_4 resulting in inner shift of Ag 3d, V 2p and O 1s orbits. The analyses distinctly indicated the presence of chemical bonds between g-C_3N_4 and Ag_3VO_4, rather than a simple physical mixture (Fig. 5).

All of the above characterization results confirmed the formation of g-C_3N_4/Ag_3VO_4 hetero-junctions.

A comparison of the optical properties for as-prepared photocatalysts using DRS is illustrated in Fig. 5. The absorbance edge of Ag_3VO_4 located at around 574 nm, and the band-gap energy revealed in the inset was approximate 2.2 eV, whereas the g-C_3N_4 sample could absorb solar energy with a wavelength shorter than 460 nm, and the band-gap energy was about 2.7 eV. With increasing g-C_3N_4 content, the absorbance edges of g-C_3N_4/Ag_3VO_4 composites showed a gradual blue shift, but the absorbance edges of all g-C_3N_4/Ag_3VO_4 hybrid materials did not obviously change. The results from DSR implied that the photocatalysts should possess visible-light photocatalytic activity.

3.2. Photocatalytic performances of the hybrid materials

The photocatalytic activities of g-C_3N_4/Ag_3VO_4 composites were evaluated by comparing degradation rates of BF under visible-light irradiation (Fig. 6).

From Fig. 6A, with the increase of visible-light irradiation time, BF was gradually decomposed by the photocatalysts. In Fig. 6B, the absorbance of BF solution showed little decrease (only 1% removal) without photocatalyst under visible-light irradiation for 2.5 h, suggesting that BF was stable and was difficult to be photolysis. After 2.5 h of visible-light irradiation, 15% of BF removal was achieved over g-C_3N_4, while the Ag_3VO_4 sample displayed a relatively high photocatalytic activity with BF degradation of 30%. All g-C_3N_4/Ag_3VO_4 photocatalysts exhibited markedly higher photocatalytic activity than that of pure g-C_3N_4 and Ag_3VO_4 under visible-light irradiation. For the hybrid photocatalysts, the photocatalytic activity was related to g-C_3N_4 content of the composites. With the increase of g-C_3N_4 content from 10 wt% to 50 wt%, the removal rate of BF was increased gradually from 60% to 95%, and then decreased to 88% under visible-light irradiation for 2.5 h. The highest degradation rate was obtained from 40 wt% g-C_3N_4/Ag_3VO_4 with 95% of BF removal.

A pseudo-first-order model was employed to investigate the kinetics of BF degradation, which is shown in Fig. S2. With increasing g-C_3N_4 content, the removal rate constant (k) first increased and then decreased (Fig. S2A). The 40 wt% g-C_3N_4/Ag_3VO_4 hybrid material exhibited optimal k value of 0.92 h^{-1}, which was 11.5 and 6.6 times higher than that of pure g-C_3N_4 and Ag_3VO_4 (Fig. S2B).

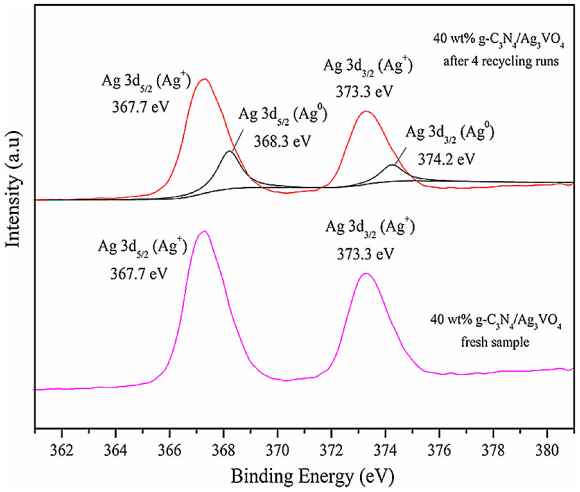

Fig. 8. XPS spectra of 40 wt% g-C_3N_4/Ag_3VO_4: after 4 recycling runs and fresh sample.

Additionally, another two typical triphenylmethane dyes of MG and CV were chosen as target pollutants to further evaluate photocatalytic activity of 40 wt% g-C_3N_4/Ag_3VO_4. Similar to BF degradation, the photocatalyst exhibited high photocatalytic activity for MG and CV removal (Fig. 7A). After 1 h irradiation with visible-light, 97% of MG degradation was achieved. Although the removal rate of CV was relatively lower than that of MG and BF, 75% of CV decomposition was still obtained under visible-light irradiation for 2.5 h. Fig. 7B reveals the change of UV–vis absorption spectra of BF, MG and CV degradation over 40 wt% g-C_3N_4/Ag_3VO_4. The characteristic peak intensity of BF (543 nm), MG (616 nm) and CV (581 nm) obviously decreased with increasing visible-light irradiation time. Moreover, with MG and CV degradation, the characteristic absorbance peak displayed a gradual blue shift. It suggested that the chromophoric structure of the dyes was decomposed. After visible-light irradiation for 1 h and 2.5 h, respectively, the main absorbance band of MG and BF almost completely disappeared. A marked decline of the main absorbance band of CV was also found under visible-light irradiation for 2.5 h.

It has been reported that some degradation intermediates are more toxic and carcinogenic than the parent dyes [28]. Prior to wastewater discharge, if dye components are completely mineralized by photocatalysts, it is highly desirable. Nevertheless, it is not easy to achieve a high mineralization rate during the photocatalytic degradation, especially under visible-light irradiation. In our work, a relatively high mineralization rate of 45% (BF), 53% (MG) and 34% (CV) was still attained by 40 wt% g-C_3N_4/Ag_3VO_4 after irradiation for 2.5 h (Fig. 7C), indicating that the three dyes were not only decolorized but also mineralized.

The stability of catalysts is very important for practical application. The transformation of Ag^+ into Ag^0 usually takes place in some Ag^+ containing semiconductors during the photocatalytic process [29]. After four recycling runs of 40 wt% g-C_3N_4/Ag_3VO_4, two Ag^0 peaks locating at 368.3 eV and 374.2 eV were found by XPS spectra (Fig. 8), respectively, suggesting that the g-C_3N_4-Ag_3VO_4-Ag composite was formed under visible-light irradiation. The photocorrosion of the catalyst might lead to a decline in photocatalytic activity. To our surprise, its photocatalytic activity did not decrease significantly after four recycling runs (Fig. 7D). A slight decline in photocatalytic activity might be from the loss of the catalyst by centrifugation.

All of the above results of BF, MG and CV degradation confirmed that the photocatalytic performances of pure g-C_3N_4 and Ag_3VO_4 could be greatly enhanced by the combination of g-C_3N_4 and Ag_3VO_4. A suitable doping amount of 40 wt% g-C_3N_4/Ag_3VO_4 could possess the highest photocatalytic activity and maintain reusability.

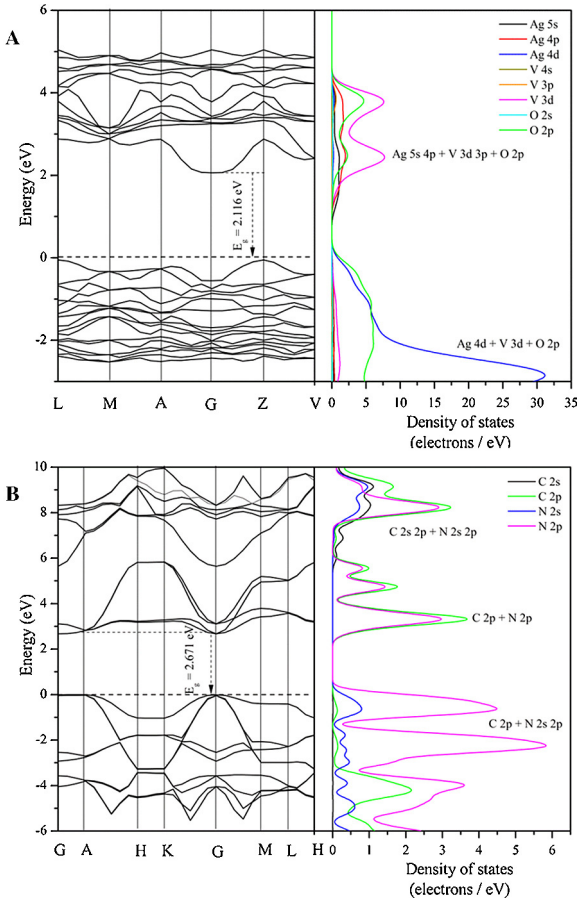

Fig. 9. The energy band structure and density of states of Ag_3VO_4 (A) and g-C_3N_4 (B).

3.3. *Mechanism of enhanced photocatalytic activity of g-C_3N_4/Ag_3VO_4 composites*

It is well known that efficient separation of electron-hole pairs is of importance for photocatalytic activity of photocatalysts [30,31]. The g-C_3N_4/Ag_3VO_4 hybrid photocatalysts exhibited much higher photocatalytic activity than that of pure g-C_3N_4 and Ag_3VO_4, indicating that photogenerated electron-hole pairs separated more efficient in the composites. In order to obtain further insight into the process, energy band structure and density of states for Ag_3VO_4 and g-C_3N_4 were calculated by density functional theory (DFT), respectively (Fig. 9). From Fig. 9A, Ag_3VO_4 was a narrow band-gap semiconductor with band-gap energy of 2.116 eV, while g-C_3N_4 had relatively wide band-gap energy of 2.671 eV (Fig. 9B). It was in good agreement with the experimental values by DSR spectra.

For Ag_3VO_4, it was important to note that the valence band (VB) edge was mainly composed of O 2p and Ag 4d orbits, while the conduction band (CB) edge was basically contributed by V 3d orbit. The much hybridization of O atoms with adjacent Ag atoms in the VB meant photoinduced electron-hole pairs from O and Ag sites. Hence, it was reasonable that the Ag_3VO_4 could provide more valence-band electrons for the CB. But the electrons were difficult to be excited. It was due to the fact that large hybrid electron density of O atoms with adjacent Ag atoms enhanced electrostatic attraction between the nuclear and electrons. Fortunately, the conduction-band electrons could easily migrate to the surface of Ag_3VO_4 to

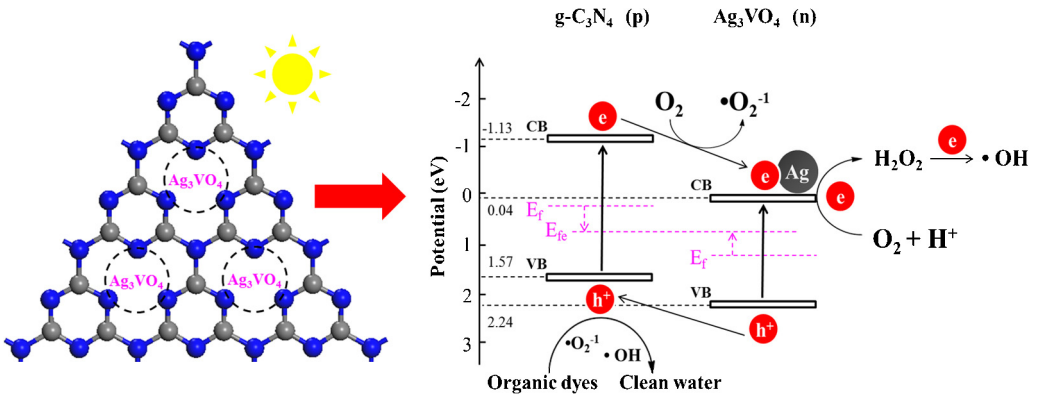

Fig. 10. Schematic diagram of electron-hole pairs' separation between p-type g-C_3N_4 and n-type Ag_3VO_4.

effectively avoid recombination of electron-hole pairs, which originated from small hybrid electron density of V atoms with adjacent Ag and O atoms in the CB reducing electrostatic attraction between the nuclear and electrons. In contrast to Ag_3VO_4, the VB edge of g-C_3N_4 was basically made up of N 2p orbit, while the CB edge consisted mainly of C 2p and N 2p orbits. The little hybridization of N atoms with adjacent C atoms in the VB implied that photogengerated electron-hole pairs only appeared at the N site and thus supplied fewer valence-band electrons to the CB. Fortunately, the electrons were easily to be excited. However, the conduction-band electrons mostly transferred inside the g-C_3N_4 to cause high recombination of electron-hole pairs owning to large hybrid electron density of C atoms with adjacent N atoms in the CB.

In the light of the above discussions, g-C_3N_4 doped Ag_3VO_4 would decrease the hybrid electron density in the VB of Ag_3VO_4, which was beneficial for valence-band electrons into the conduction band. Similarly, the introduction of Ag_3VO_4 would also cause the decline of hybrid electron density in the CB of g-C_3N_4, which favored conduction-band electrons to transfer to the surface of Ag_3VO_4 and thereby hindered recombination of electron-hole pairs. Therefore, the combination of Ag_3VO_4 and g-C_3N_4 could increase separation efficiency of electron-hole pairs and thus enhance photocatalytic activity of g-C_3N_4/Ag_3VO_4 hybrid photocatalysts.

The enhanced photocatalytic activity can be also ascribed to the formation of hetero-junction between p-type g-C_3N_4 and n-type Ag_3VO_4. The conduction band-edge energy of a semiconductor can be predicted by Mulliken electronegativity theory.

$$E_{CB} = \chi - E^c - 0.5E_g$$

Herein, E_{CB} is the conduction band-edge energy. The χ is the absolute electronegativity of the semiconductor, which is the geometric mean of the electronegativity of the constituent atoms. E^c is the energy of free electrons in the hydrogen scale (about 4.5 eV). E_g is the band-gap energy of the semiconductor. The valence band-edge energy can be obtained by $E_{VB} = E_{CB} + E_g$. The χ value for Ag_3VO_4 is 5.64 eV. Consequently, the E_{CB} value of Ag_3VO_4 was calculated to be 0.04 eV/NHE, and the E_{VB} value was estimated to be 2.24 eV/NHE. Based on the band-gap positions, the CB and VB edge energies of g-C_3N_4 were predicted to be −1.13 and 1.57 eV/NHE, respectively, which was in line with previous report [16]. The photogenerated electrons on the conduction band of p-type g-C_3N_4 could transfer to Ag and then transfer to n-type Ag_3VO_4 [32]. Meanwhile, photoinduced holes could migrate from the valence band of n-type Ag_3VO_4 to that of p-type g-C_3N_4. With the transfer of electrons and holes, the Fermi level (E_f) of p-type g-C_3N_4 moved down, while that of n-type Ag_3VO_4 moved up until the equilibrium state (E_{fe}) was achieved. An inner electric field from n-type Ag_3VO_4 to p-type g-C_3N_4 was established, which greatly promoted separation of electron-hole pairs in the hetero-junction [10,13]. It was in good agreement with band-edge hybridization by DFT calculations.

According to the above investigations, electron-hole pairs' separation in the hetero-junction under visible-light irradiation was proposed in Fig. 10.

In order to prove above-proposed mechanism, electron-hole pairs' recombination for g-C_3N_4, Ag_3VO_4 and 40 wt% g-C_3N_4/Ag_3VO_4 was detected by photoluminescence technique. The fluorescence intensity with higher value means more recombination of electron-hole pairs and lower photocatalytic activity. As shown in Fig. 11, pure g-C_3N_4 excited at 350 nm had a strong emission peak at about 460 nm. For pure Ag_3VO_4, the emission intensity was much lower than that of pure g-C_3N_4 at similar emission position. The PL spectra of 40 wt% g-C_3N_4/Ag_3VO_4 was similar to pure Ag_3VO_4, but its peak intensity obviously decreased. The PL results distinctly demonstrated that the recombination ability of electron-hole pairs was g-C_3N_4 > Ag_3VO_4 > 40 wt% g-C_3N_4/Ag_3VO_4, which confirmed the results of theoretical calculations.

3.4. Investigation of reactive species

As we all know, dyes are decomposed by photocatalysts under light irradiation, which is mainly ascribed to generate reactive species such as h^+, $\bullet O_2^{-1}$ and •OH, and so on [33–36]. In this study, $\bullet O_2^{-1}$ involved in the photodegradation could be formed by $O_2 + e = \bullet O_2^{-1}$, which was primarily due to more negative reduction potential of g-C_3N_4 (E_{CB} = −1.13 eV)

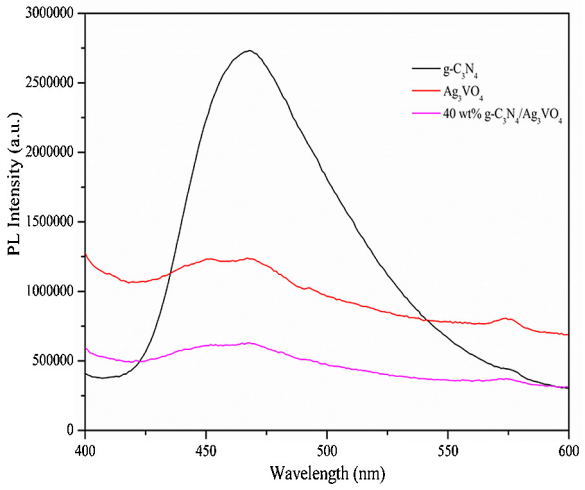

Fig. 11. Photoluminescence spectra of g-C_3N_4, Ag_3VO_4 and 40 wt% g-C_3N_4/Ag_3VO_4.

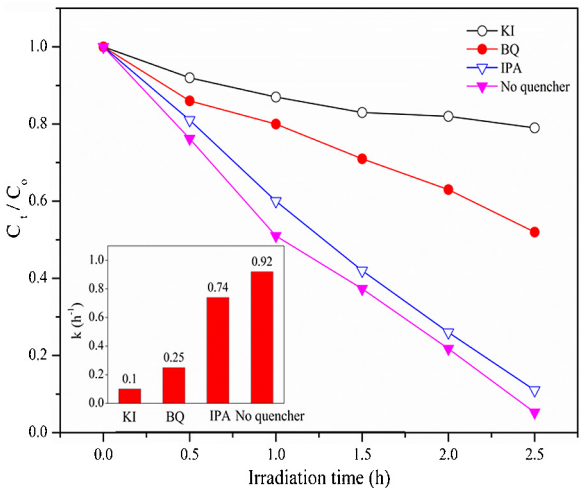

Fig. 12. Photocatalytic activity of 40 wt% g-C_3N_4/Ag_3VO_4 for BF with different scavenges under visible-light irradiation.

compared with $O_2/{\bullet}O_2^{-1}$ ($E^0(O_2/{\bullet}O_2^{-1}) = -0.33$ eV/NHE) [37]. In addition, •OH produced in solution might be from the following reactions: $O_2 + 2e^- + 2H^+ = H_2O_2$, $H_2O_2 + e = {\bullet}OH + OH^-$. Because reduction potential of O_2/H_2O_2 was 0.695 eV [37], it was reasonable that O_2 reacted with electrons and hydrogen ions to produce H_2O_2. Subsequently, H_2O_2 captured electrons to generate •OH in solution. The adsorbed •OH in the photocatalytic degradation could not be produced because of more positive oxidation potential of 2.72 eV/NHE (•OH, H^+/H_2O) [38] compared to g-C_3N_4 (E_{VB} = 1.57 eV) and Ag_3VO_4 (E_{VB} = 2.24 eV). Thus, the photoinduced holes could not oxidize H_2O to form adsorbed •OH on the surface of g-C_3N_4/Ag_3VO_4.

In order to detect the above-mentioned three reactive species, different scavenges of KI (h^+ and •OH quencher), benzoquinone (BQ, $\bullet O_2^{-1}$ quencher) and 2-propanol (IPA, •OH quencher) were introduced in the process of BF degradation. The dosages referred to previous studies [38,39]. From Fig. 12, KI added into BF solution leaded to a great decrease of the removal rate constant (k) from 0.92 h^{-1} to 0.1 h^{-1}. The removal rate constant (k) also had an obvious drop to 0.25 h^{-1} in the presence of BQ. Additionally, 2-propanol showed little effect on the k of BF degradation. The results proved existence of the three reactive species. However, h^+ and $\bullet O_2^{-1}$ were two main reactive species in the photocatalytic process.

4. Conclusions

In this work, an enhanced visible-light-driven photocatalyst of g-C_3N_4/Ag_3VO_4 by the combination of g-C_3N_4 and Ag_3VO_4 was designed. Among hybrid photocatalysts, the 40 wt% g-C_3N_4/Ag_3VO_4 sample exhibited optimal photocatalytic activity for BF degradation under visible-light irradiation. Furthermore, the photocatalyst could also efficiently remove other organic dyes such as malachite green and crystal violet in wastewater. In addition, the reusability experiments suggested that the photocatalytic material possessed good stability. In general, the Ag_3VO_4 hybridized with g-C_3N_4 could address the problem of low photocatalytic activity of g-C_3N_4 and Ag_3VO_4 used alone. This work might provide a promising approach for treatment of dye wastewater.

Acknowledgments

The authors greatly acknowledge the National Natural Science Foundation of China (No. 21177055 and 51278242) for financial support. The present research was also supported by Jiangsu Provincial Science and Technology Supporting Program (No. BE2012116).

Appendix A. Supplementary data

Supplementary data associated with this article can be found, in the online version, at http://dx.doi.org/10.1016/j.apcatb.2013.08.008.

References

[1] J.C. Greene, G.L. Baughman, Text. Chem. Color. 28 (1996) 23–30.
[2] M.D. Hernando, S. De Vettori, M.J. Martinez Bueno, A.R. Fernandez-Alba, Chemosphere 68 (2007) 724–730.
[3] H. Lachheb, E. Puzenat, A. Houas, M. Ksibi, E. Elaloui, C. Guillard, J.M. Herrmann, Appl. Catal. B 39 (2002) 75–90.
[4] H.X. Li, Z.F. Bian, J. Zhu, D.Q. Zhang, G.S. Li, Y.N. Huo, H. Li, Y.F. Lu, J. Am. Chem. Soc. 129 (2007) 8406–8407.
[5] T. Hirakawa, P.V. Kamat, J. Am. Chem. Soc. 127 (2005) 3928–3934.
[6] M.J. Height, S.E. Pratsinis, O. Mekasuwandumrong, P. Praserthdam, Appl. Catal. B 63 (2006) 305–312.
[7] C. Pan, Y. Zhu, J. Mater. Chem. 21 (2011) 4235–4241.
[8] A. Kudo, K. Omori, H. Kato, J. Am. Chem. Soc. 121 (1999) 11459–11467.
[9] S. Tokunaga, H. Kato, A. Kudo, Chem. Mater. 13 (2001) 4624–4628.
[10] X. Li, R. Huang, Y. Hu, Y. Chen, W. Liu, R. Yuan, Z. Li, Inorg. Chem. 51 (2012) 6245–6250.
[11] H.F. Cheng, B.B. Huang, Y. Dai, X.Y. Qin, X.Y. Zhang, Langmuir. 26 (2010) 6618–6624.
[12] X. Xiao, W.D. Zhang, J. Mater. Chem. 20 (2010) 5866–5870.
[13] G.P. Dai, J.G. Yu, G. Liu, J. Phys. Chem. C 115 (2011) 7339–7346.
[14] Z. Yi, J. Ye, N. Kikugawa, T. Kako, S. Ouyang, H. Stuart-Williams, H. Yang, J. Cao, W. Luo, Z. Li, Y. Liu, R.L. Withers, Nat. Mater. 9 (2010) 559–564.
[15] Y.P. Bi, H.Y. Hu, S.X. Ouyang, G.X. Lu, J.Y. Cao, J.H. Ye, Chem. Commun. 48 (2012) 3748–3750.
[16] X. Wang, K. Maeda, A. Thomas, K. Takanabe, G. Xin, J.M. Carlsson, K. Domen, M. Antonietti, Nat. Mater. 8 (2009) 76–80.
[17] J. Hu, W. Cheng, S. Huang, D. Wu, Z. Xie, Appl. Phys. Lett. 89 (2006).
[18] Q.J. Xiang, J.G. Yu, M. Jaroniec, J. Phys. Chem. C 115 (2011) 7355–7363.
[19] S.C. Yan, Z.S. Li, Z.G. Zou, Langmuir. 25 (2009) 10397–10401.
[20] S.C. Yan, Z.S. Li, Z.G. Zou, Langmuir. 26 (2010) 3894–3901.
[21] G. Liu, P. Niu, C. Sun, S.C. Smith, Z. Chen, G.Q. Lu, H.-M. Cheng, J. Am. Chem. Soc. 132 (2010) 11642–11648.
[22] R. Konta, H. Kato, H. Kobayashi, A. Kudo, Phys. Chem. Chem. Phys. 5 (2003) 3061–3065.
[23] H. Xu, J. Yan, Y. Xu, Y. Song, H. Li, J. Xia, C. Huang, H. Wan, Appl. Catal. B 129 (2013) 182–193.
[24] S. Matsumoto, E.Q. Xie, F. Izumi, Diamond Relat. Mater. 8 (1999) 1175–1182.
[25] Y.J. Wang, R. Shi, J. Lin, Y.F. Zhu, Energy Environ. Sci. 4 (2011) 2922–2929.
[26] L. Qi, J. Yu, M. Jaroniec, Phys. Chem. Chem. Phys. 13 (2011) 8915–8923.
[27] A. Thomas, A. Fischer, F. Goettmann, M. Antonietti, J.-O. Mueller, R. Schloegl, J.M. Carlsson, J. Mater. Chem. 18 (2008) 4893–4908.
[28] L.A. Perez-Estrada, A. Agueera, M.D. Hernando, S. Malato, A.R. Fernandez-Alba, Chemosphere 70 (2008) 2068–2075.
[29] W. Liu, X. Liu, Y. Fu, Q. You, R. Huang, P. Liu, Z. Li, Appl. Catal. B 123 (2012) 78–83.
[30] Y. Wang, X. Bai, C. Pan, J. He, Y. Zhu, J. Mater. Chem. 22 (2012) 11568–11573.
[31] J. Fu, Y. Tian, B. Chang, F. Xi, X. Dong, J. Mater. Chem. 22 (2012) 21159–21166.
[32] Q. Zhu, W.S. Wang, L. Lin, G.Q. Gao, H.L. Guo, H. Du, A.W. Xu, J. Phys. Chem. C 117 (2013) 5894–5900.
[33] L.-S. Zhang, K.-H. Wong, H.-Y. Yip, C. Hu, J.C. Yu, C.-Y. Chan, P.-K. Wong, Environ. Sci. Technol. 44 (2010) 1392–1398.
[34] K. Yu, S. Yang, C. Liu, H. Chen, H. Li, C. Sun, S.A. Boyd, Environ. Sci. Technol. 46 (2012) 7318–7326.
[35] M. Yin, Z. Li, J. Kou, Z. Zou, Environ. Sci. Technol. 43 (2009) 8361–8366.
[36] X. Lin, T. Huang, F. Huang, W. Wang, J. Shi, J. Phys. Chem. B 110 (2006) 24629–24634.
[37] J. Kim, C.W. Lee, W. Choi, Environ. Sci. Technol. 44 (2010) 6849–6854.
[38] G. Li, K.H. Wong, X. Zhang, C. Hu, J.C. Yu, R.C.Y. Chan, P.K. Wong, Chemosphere 76 (2009) 1185–1191.
[39] H. Lin, J. Cao, B. Luo, B. Xu, S. Chen, Catal. Commun. 21 (2012) 91–95.